BNL-105597-2014-TECH

BNL/SNS Technical Note No. 028;BNL-105597-2014-IR

Fast Transverse Instability in the NSNS Accumulator Ring

A. G. Ruggiero

April 1997

Collider Accelerator Department

Brookhaven National Laboratory

U.S. Department of Energy

USDOE Office of Science (SC)

DISCLAIMER

FAST TRANSVERSE INSTABILITY
in the NSNS ACCUMULATOR RING

BNL/NSNS TECHNICAL NOTE

NO. 028

A. G. Ruggiero and M. Blaskiewicz

April 24, 1997

ALTERNATING GRADIENT SYNCHROTRON DEPARTMENT
BROOKHAVEN NATIONAL LABORATORY
UPTON, NEW YORK 11973

Fast Transverse Instability in the NSNS Accumulator Ring*

A. G. Ruggiero and M. Blaskiewicz
Brookhaven National Laboratory

April 24, 1997

Introduction

This technical note reports on the results of investigation of possible fast transverse instabilities in the NSNS Accumulator Ring. The instability may be caused by the presence of stripline devices like kicker magnets, the active damper system, and by the RF cavities, and the sharp steps of the vacuum pipe. Conventional formulae that can be found in the literature have been used, some of them with arguable validity, as they will be discussed in the report. The instability can be overcome by adopting aluminum as the material of the vacuum chamber, and by smoothing the shape of the vacuum pipe. The resistive contribution to the coupling impedance from the RF cavities, the kicker magnets and other striplines devices in the ring has to be maintained under control with careful engineering design. Still the growth time of the instability remains short especially for the mode in proximity of the betatron tune. The growth rate can be lowered by a factor of four if the fractional part of the tune is shifted from 0.8 to 0.2.

The NSNS Accumulator Ring

The function of the Accumulator Ring is to take the 1.0 GeV proton beam from the Linac and convert the long Linac beam pulse of about 1 ms into a 0.5 microsecond beam in about 1280 turns. The bunch compression occurs during the injection process, and the beam is immediately extracted at the end of the process. The final beam has an intensity of 2.08×10^{14} proton per pulse, resulting in 2 MW average beam power at 60 Hz repetition rate. The lattice of the Accumulator Ring is a simple FODO lattice with four-fold symmetry [1], and the dispersion function is reduced to zero at straight sections by the missing magnet scheme. The total circumference of the ring is 220.7 m and the transition energy is $\gamma_T = 4.93$, higher than the operating energy of 1 GeV. The salient design parameters are shown in Table 1.

The Ring Vacuum Pipe

The main parameters that enter the investigation of the coherent transverse instability are the dimension and the shape of the vacuum chamber, and the resistivity of the wall. The NSNS Accumulator Ring is made of three different sections: (i) The region of bending magnets where the shape of the vacuum pipe is rectangular with internal dimensions of 23 cm (H) and 13 cm (V). This region is expected to cover about 25 % of the whole ring circumference. (ii) The region of

* Work performed under the auspices of the U.S. Department of Energy

small quadrupoles where the vacuum pipe is circular with the internal diameter of 2b = 18 cm. This region is expected to cover about 60 % of the ring circumference. (iii) The region of large quadrupoles where also the pipe is circular but the internal diameter is 2b = 14 cm. This region covers the remaining 15 % of the circumference.

It is not clear at this moment how the sections of different shape are to be joined to each other. There are two solutions: one makes use of sharp transitions, and the other one of tapered connections from one shape to the other. The analysis that was made uses formulae that apply strictly to circular geometry. Thus we have approximated the rectangular vacuum chamber by a circular one with an internal diameter given by $2b = (H + V) / 2 = 18$ cm. By taking an average of the pipe dimension around the ring we have then assumed a pipe with an internal radius b = 10 cm. For most of the chamber components entering the analysis, it is indeed sufficient to specify a single shape and a single dimension. The analysis of the vacuum pipe steps, of course, require more details about the transitions.

Table 1: General Parameters of the NSNS Accumulator Ring

Average Power	2 MW
Kinetic Energy	1.0 GeV
Circumference, $2\pi R$	220.7 m
Bending Field	7.4 kG
Number of Protons, N	2.08×10^{14}
Betatron Tunes, $Q_{H/V}$	5.8 / 5.8
Transition Energy, γ_T	4.93
Natural Chromaticity, $\xi_{H,V}$	-6.50, -7.29
Full Betatron Emittance, ε_{tot}	$120\ \pi$ mm mrad
Space-Charge Tune-Shift	< 0.2
RF peak Voltage (h=1)	42 kV
Revolution Frequency	1.1887 MHz
Filling Time	1.018 ms
Synchrotron Period, T_s	0.9 ms
Bunching Factor, B	0.325
Total Bunch Area, S	10 eV-s
Full Bunch Length, L	546.6 ns
Full Momentum Spread, Δ	1.6 %
Average Beam radius, a	3.80 cm
Average Pipe Radius, b	10 cm

The material of the vacuum chamber can be either stainless steel with a surface resistivity of $\rho_w = 73\ \mu\Omega$ x cm, or aluminum with $\rho_w = 2.83\ \mu\Omega$ x cm. The vacuum system may require stainless steel for rigidity of the vacuum chamber and to avoid electron desorption at the wall. On the other end, the resistive wall instability may be softened by employing a higher conductor like aluminum. It may be also quite possible that a mixture of the two materials are used around the circumference.

Transverse Beam Dimension

The betatron emittance quoted in Table 1 defines the total beam, that is 100% of it. It has the same value in the two planes of oscillation. We shall adopt the criterion to define the total emittance ε_{tot} as 5 times the rms emittance ε_{rms}. Define the average values of the envelope functions $<\beta_{H,V}> = R / Q_{H,V}$, with R the average closed orbit radius and $Q_{H,V}$ the betatron tunes. The average rms beam size in the vertical and horizontal plane are given by $\sigma_{H,V} = (<\beta_{H,V}> \varepsilon_{rms})^{1/2}$. This is the contribution from the betatron motion alone, to which we should add the contribution in the horizontal plane from the relative momentum spread δ in the beam, which is $\sigma_E = <\eta> \delta$, where $<\eta> = R / \gamma_T^2$ is the average value of the dispersion around the ring. The total beam relative momentum spread Δ is given in Table 1. The rms value δ is 1/5 of the full value.

It is sometime required to specify the average full beam radius around the ring. The assumption commonly made is that the beam has a transverse uniform charge distribution and a circular shape with radius a, which we estimate as $a = 3 [\sigma_V (\sigma_H^2 + \sigma_E^2)^{1/2}]^{1/2}$

Longitudinal Beam Dimension

The total bunch area is S = 10 eV-s. We shall assume a single RF cavity system for the bunch compression. The requirement is a beam gap, free of any particles, of 294.7 ns and a full bunch length L = 546.6 ns. Assuming again, as usual, a ratio of factor 5 between total and rms values, we can estimate the rms bunch length σ and rms momentum spread δ. The RF system operates at the harmonic number h = 1, and there is thus a single beam bunch, which we assume to hold a cos square distribution. We can then also estimate the bunching factor according to the formula $B = 0.5\ L\ f_0$, where f_0 is the revolution frequency. All the other salient parameters describing the beam longitudinal dimension and longitudinal motion are given in Table 1.

Time Dependence of the Beam Dimensions

We shall assume that the bunch length remains unchanged during the multi-turn injection process, whereas the beam intensity varies linearly with time. At the same time, it is also a good approximation to assume that the beam emittance increases linearly with time, eventually with the help of some "painting" technique, so that the ratio N/ε is constant during the injection process. Thus, the actual beam size will increases with the square root of the beam intensity. The beam is immediately extracted at the end of the injection process, and a proton will spend circulating in the ring at most 1.0 ms. The parameters listed in Table 1 correspond to the end of the injection process.

The Fast Transverse Instability

It is seen from Table 1 that the synchrotron period is 0.9 ms, so that the beam bunch will complete only one full synchrotron oscillation before it is extracted. The growth rate of any transverse instability, in order to have a consequence to the beam disruption and loss, will have to be considerably larger than the synchrotron frequency. This situation is characterized as a fast transverse instability, where the synchrotron motion can be neglected and the beam bunch can be treated as a chopped section of coasting beam. The well-known coasting beam theory [2,3] of transverse coherent instability can then be applied.

A coherent perturbation may develop around the contour of the beam bunch. The wavelength of this perturbation has to be at least the bunch length, if not smaller. This sets a lower limit to the perturbation frequency. In terms of the revolution harmonic number this limit is $n > 5$, that is larger than the betatron tune. The upper limit is set by the cut-off due to the presence of the vacuum chamber which is given by $n < \gamma R/b \sim 726$ for a circular pipe of 20 cm diameter. Outside this range a transverse coherent instability cannot be expected.

The Theory of Transverse Coherent Instabilities for Coasting Beams

The stability condition for this type of coherent motion is

$$| Z_T | < E_0 \pi Q_{H,V} \beta \gamma [| (n - Q_{H,V}) \eta + \xi_{H,V} | (\Delta p/p) + \delta v] / e I_p R = Z_{beam} \qquad (1)$$

where $\Delta p/p$ is the FWHM value of the beam momentum spread which is about half of the value of the full momentum spread Δ, E_0 is the proton rest energy, $\xi_{H,V}$ the chromaticity of the Accumulator Ring, and δv the betatron tune spread from non linear elements like octupole magnets. I_p is the peak current of the bunch

$$I_p = Ne / (2 \pi)^{1/2} \sigma \qquad (2)$$

To the left of the inequality (1) we have the transverse coupling impedance Z_T which will be discussed below. It describes the electromagnetic interaction between the beam and the surrounding.

In absence of Landau damping, that is of a sufficiently large spread of betatron frequencies within the beam bunch, one can estimate the growth rate of the coherent instability

$$\tau^{-1} = I_p r_p \mathrm{Re} (Z_T) / e Q_{H,V} \gamma Z_0 \qquad (3)$$

where $Z_0 = 377$ ohm, and $r_p = 1.535 \times 10^{-18}$ m, the classical proton radius.

As we shall see below, we are indeed in a case where the space charge contribution to the coupling impedance dominates. The frequency of the coherent instability, usually in proximity of a betatron sideband, will suffer a large shift. This is an indication that there is no Landau damping naturally built within the beam large enough to compensate for the shift, unless this is introduced externally, for instance, with large octupolar magnetic field. In any case the real frequency shift of the coherent instability is given by

$$\Delta\omega \;=\; I_p\, r_p\, \mathrm{Im}\,(\, Z_T\,) \,/\, e\, Q_{H,V}\, \gamma\, Z_0 \qquad (3)$$

The Transverse Coupling Impedance

There are four major contributions [4] to the transverse coupling impedance. The space-charge contribution dominates in a low-energy storage ring:

$$Z_T \;=\; i\, R\, Z_0\, (\, a^{-2} - b^{-2}\,) \,/\, \beta^2 \gamma^2. \qquad (4)$$

Next, we have the contribution from the wall resistivity:

$$Z_T \;=\; (\, 1 - i\,)\, R\, [\, 2\, R\, Z_0\, \rho_W \,/\, \beta\, (\, n - Q_{H,V}\,)\,]^{1/2} \,/\, b^3. \qquad (5)$$

By virtue of the deflection theorem [4], the longitudinal coupling impedance Z/n can be translated into an equivalent transverse coupling impedance:

$$Z_T \;=\; 2\, R\, Z \,/\, \beta\, b^2\, (\, n - Q_{H,V}\,). \qquad (6)$$

The wall components included in the deflection mode analysis are: bellows, striplines for the beam position monitors and the active damper system, kicker magnets, vacuum chamber steps, vacuum ports, and RF cavities [5]. Finally, there are transverse (as well longitudinal) parasitic modes due to several resonating structures, which are difficult to estimate, but that can be calculated with codes like MAFIA, or measured with the wire method or with the beam itself.

A large contribution to the real part of the impedance comes from the resistivity of the wall and from the vacuum chamber steps. The impedance varies with the square root of the wall resistivity. By adopting aluminum instead of stainless steel, one can reduce the impedance by a factor of five. The steps of the vacuum chamber require a more involved analysis. The longitudinal coupling impedance from M single steps (uncoupled) was estimated some time ago by H. Hereward [6]

$$Z/n \;=\; 2\, M\, (\, L - i\pi\,)\, Z_0\, (\, W - 1\,)^2\, b \,/\, 2\, \pi^2\, R \qquad (7)$$

for $n < n_W \;=\; 2\pi R \,/\, 2b\, (\, W - 1\,)$, and for $n > n_W$

$$Z/n \;=\; Z_0\, M\, (\, W - 1\,) \,/\, 2\pi n \qquad (8)$$

where $W = b_2 / b_1$ is the ratio of the outer dimension b_2 to the inner dimension b_1 of the step.

According to this formula a substantial resistive contribution occurs in the low frequency range. It is associated to the actual energy loss suffered by a charged particle due to the diffraction phenomenon of an electro-magnetic plane wave being scattered by discontinuities. One should point out that very likely the result really applies only to wavelengths which have about the pipe dimension, that is in the proximity of the cut-off. Moreover, steps come in pair, an entrance followed by an exit discontinuity. Thus, one deals in reality with resonating cavities rather than single de-coupled steps. A step could be treated as a single discontinuity only at those wavelengths that are considerably shorter than the separation between the steps. The contribution represented by Eq.s (7 and 8) has been originally included in the analysis also for very low frequencies, but we believe that otherwise it should really not be included. In any event, we have assumed 32 pairs of steps separated by about 2 m, with an inner radius of 10 cm and an outer radius of 13 cm. A simulation with ABCI [7] of a pair of such transitions have shown the results of Figure 1. It is indeed seen that no resistive contribution is noticeable up to about the pipe cutoff frequency.

Though it was clearly demonstrated that relation (6) between longitudinal and transverse coupling impedance holds well for stripline devices, like beam position monitors, kickers and the damper system [8], there are some questions about its validity for cavity-like objects, like bellows, vacuum chamber steps, vacuum ports, and RF cavities. Nonetheless, also for these components we have calculated the longitudinal coupling impedance [5] and have then derived the transverse coupling impedance in combination with Eq.(6). The results are displayed in Tables 2 to 11. The impedance of each component has been adjusted by taking into account cutoff functions which are shown in Table 2. The summary of individual contributions and of the totals are shown in Tables 12 and 13. Figure 2 is the display of the total expected transverse coupling impedance versus the harmonic number n for the NSNS Accumulator Ring.

Results for the NSNS Accumulator Ring

Figure 2 is the plot of the transverse coupling impedance versus the harmonic number. The peak around n = 6 is caused by the dependence with the betatron tunes as shown both in Eq. (5) for the resistive wall contribution and in Eq. (6) for the deflection modes. To determine the stability of the beam, we plot the difference $|Z_T| - Z_{beam}$ in Figure 3, taking $\delta\nu = 0$. It is seen that the beam is unstable for all modes n < 100. The instability is caused essentially by the large value of the space charge, the contribution of which to the total impedance dominates. It was determined that damping from the natural chromaticity is not effective. The beam is stable for large mode numbers as a consequence of the frequency compaction factor η.

The growth time τ of the instability, in absence of Landau damping, is plotted in Figure 4. The minimum is $\tau = 5.3$ μs for n = 6. At n = 7 the growth time $\tau = 40$ μs, and at n = 8, $\tau = 91$ μs. The ratio of the synchrotron period T_s to the growth time τ is plotted in Figure 5. It shows that we are indeed dealing with a fast transverse instability for those harmonics in proximity of the betatron tune. In this case, the longitudinal motion can be entirely neglected.

Finally, Figure 6 is the plot of the real frequency shift $\Delta\omega$, divided by the angular revolution frequency $2\pi f_0$, versus the harmonic number n. It is seen that the shift is only a small fraction of one harmonic. Thus the possibility of overlapping of neighboring stopbands (mode coupling) seems to be excluded in the NSNS Accumulator Ring. Moreover, $\Delta\omega / 2\pi f_0$ is about the amount of tune spread which is required to make the motion stable. This tune spread, for instance, can be introduced with octupole magnets. It is seen that the required tune spread is less than or at most $\Delta\nu = 0.1$ for all modes, except for n = 6 when $\Delta\nu = 0.2$.

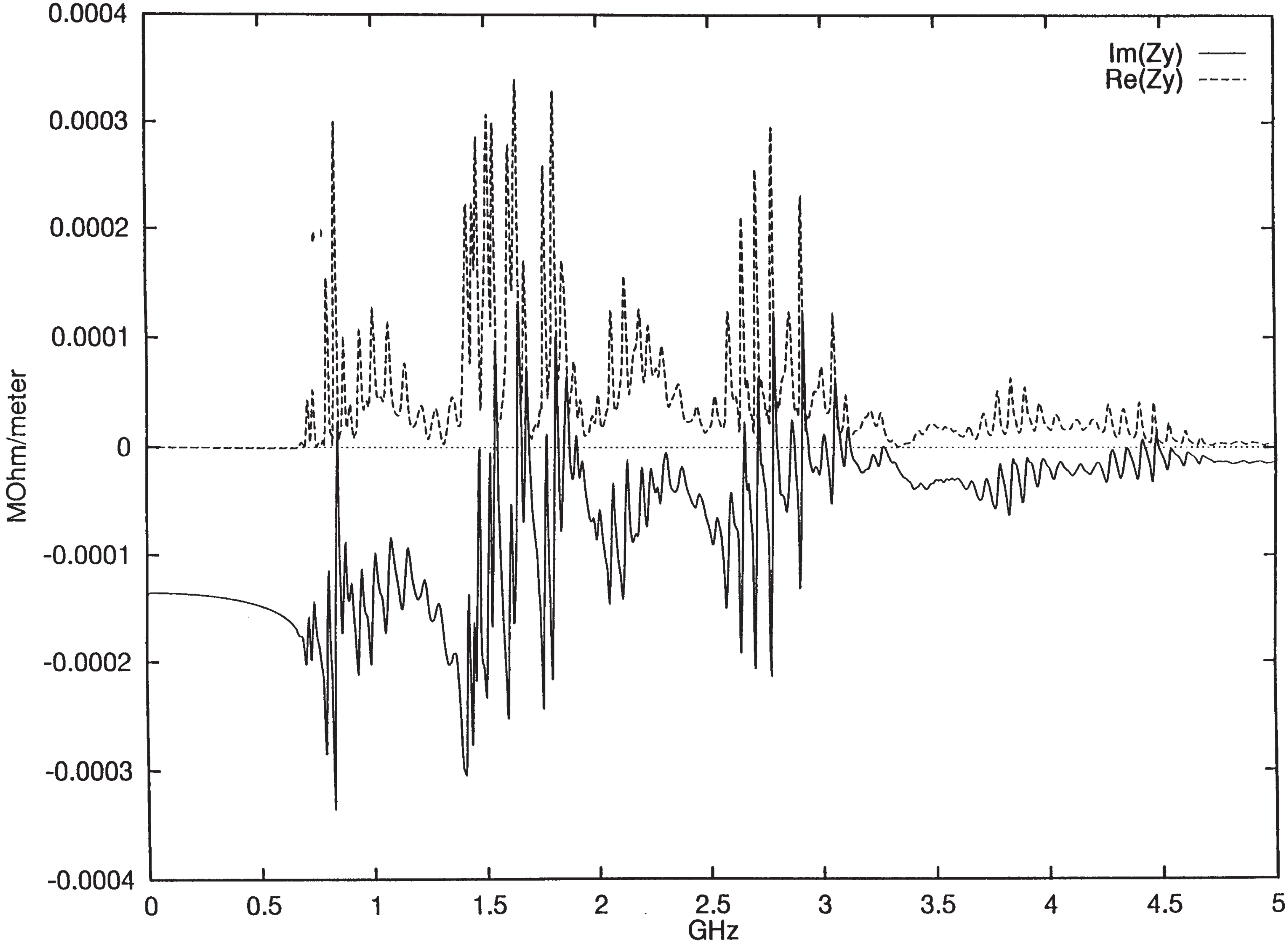

Figure 1. Transverse Coupling Impedance of a pair of Circular Transitions from 10 to 13 cm, 2 meter apart.

Table 2: Cutoff Functions

Pipe Radius, b	10 cm	
Beam Size, a	37.9615743 mm	
a/b	0.37961574	
γ	2.06580266	
Pipe cutoff	726	610.763268 MHz

n	Cut-Off Space-Charge	Cut-Off Pipe	$nb/\gamma R$
1	0.99999986	0.99999905	0.00137741
2	0.99999945	0.99999621	0.00275482
3	0.99999877	0.99999146	0.00413223
4	0.99999781	0.99998482	0.00550964
5	0.99999658	0.99997628	0.00688705
6	0.99999508	0.99996585	0.00826446
7	0.9999933	0.99995352	0.00964187
8	0.99999125	0.99993929	0.01101928
9	0.99998893	0.99992316	0.01239669
10	0.99998633	0.99990514	0.0137741
20	0.99994532	0.99962062	0.02754821
30	0.99987697	0.9991466	0.04132231
40	0.9997813	0.99848334	0.05509642
50	0.9996583	0.99763124	0.06887052
60	0.99950798	0.99659076	0.08264463
70	0.99933037	0.9953625	0.09641873
80	0.99912547	0.99394716	0.11019284
90	0.9988933	0.99234554	0.12396694
100	0.99863388	0.99055855	0.13774105
200	0.99454671	0.96276571	0.27548209
300	0.98777191	0.91816636	0.41322314
400	0.97836464	0.85917662	0.55096419
500	0.9664011	0.78886707	0.68870523
600	0.95197749	0.71069869	0.82644628
700	0.93520869	0.62824278	0.96418733
800	0.91622679	0.5449163	1.10192837
900	0.89517929	0.46375906	1.23966942
1000	0.87222728	0.3872713	1.37741047

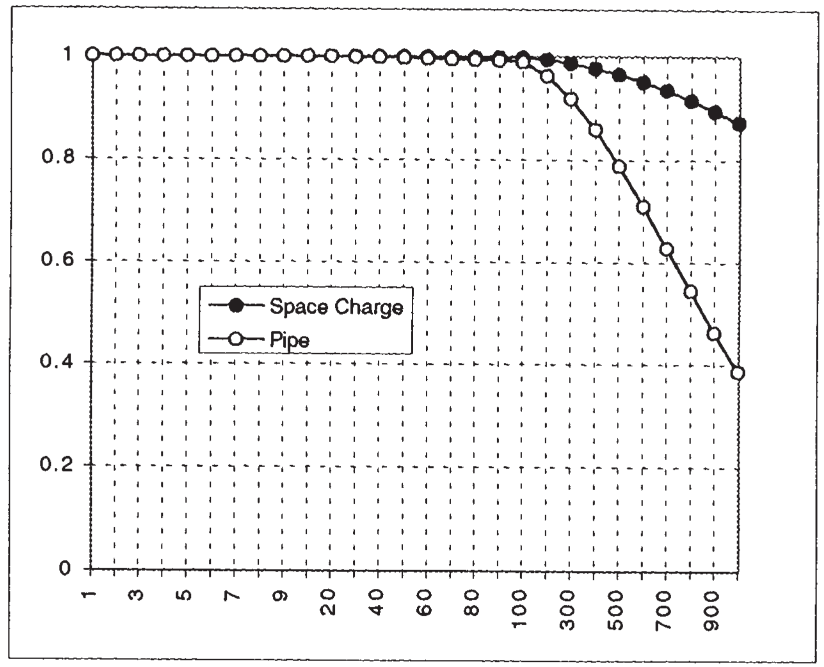

Table 3: Space-Charge Transverse Coupling Impedance (kohm/m)

Pipe Radius, b	10 cm
Beam Size, a	37.9615743 mm
β	0.87502743
γ	2.06580266
Circumference	220.688 m
Z_Trans	2406.85367 khom/m

n	Real	Imaginary
1	0	2406.85334
2	0	2406.85236
3	0	2406.85071
4	0	2406.84841
5	0	2406.84545
6	0	2406.84183
7	0	2406.83755
8	0	2406.83262
9	0	2406.82702
10	0	2406.82077
20	0	2406.72207
30	0	2406.55757
40	0	2406.32728
50	0	2406.03124
60	0	2405.66946
70	0	2405.24197
80	0	2404.74881
90	0	2404.19001
100	0	2403.56563
200	0	2393.72841
300	0	2377.42244
400	0	2354.78052
500	0	2325.98604
600	0	2291.27052
700	0	2250.91048
800	0	2205.22381
900	0	2154.56557
1000	0	2099.32343

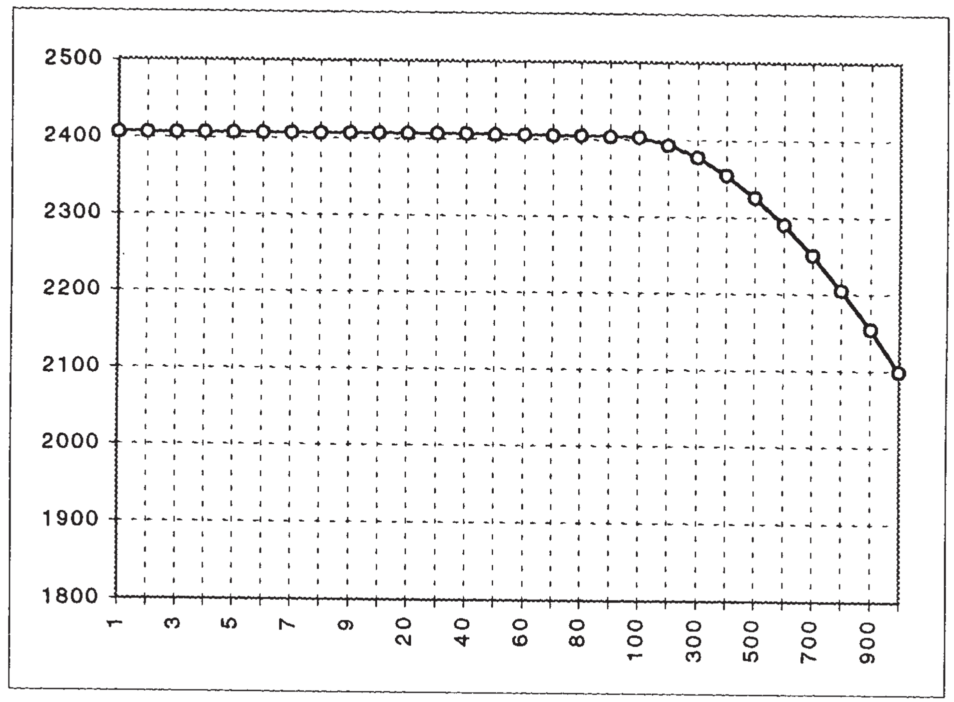

Table 4: Resistive-Wall Transverse Coupling Impedance (kohm/m)

Circumference	220.688 m			
Average Radius	35.1235861 m			
Material	Stainless Steel	Copper	Aluminum	
Resistivity	73	1.8	2.83	μohm-cm
Fraction	**0.15**	**0**	**0.85**	
Skin Depth	0.91616775	0.14386323	0.18038764	mm @ $n = Q_{H,V}$
β	0.87502743			
Average Wall Resistivity	3.687175 μohm-cm			
Vacuum Chamber Thickness	**5** mm			
Pipe Radius	10 cm			
$Q_{H,V}$	5.82			
Z-Trans @ $n=Q_{H,V}$	2.76556416	-2.7655642 kohm/m		$(n-Q_{H,V})^{-1/2}$
$n-Q_{H,V}$	0.18			

n	Real	Imaginary
1	0.53443644	-0.5344364
2	0.60032532	-0.6003253
3	0.69870159	-0.6987016
4	0.86971649	-0.8697165
5	1.29569495	-1.2956949
6	2.76546972	-2.7654697
7	1.08008715	-1.0800872
8	0.79463077	-0.7946308
9	0.65791996	-0.65792
10	0.57383978	-0.5738398
20	0.31147062	-0.3114706
30	0.23840813	-0.2384081
40	0.20038942	-0.2003894
50	0.17610722	-0.1761072
60	0.15886102	-0.158861
70	0.14578116	-0.1457812
80	0.13540661	-0.1354066
90	0.12690492	-0.1269049
100	0.11976249	-0.1197625
200	0.08106593	-0.0810659
300	0.06281087	-0.0628109
400	0.05077561	-0.0507756
500	0.04163717	-0.0416372
600	0.03420948	-0.0342095
700	0.02797766	-0.0279777
800	0.02268769	-0.0226877
900	0.01819701	-0.018197
1000	0.01441129	-0.0144113

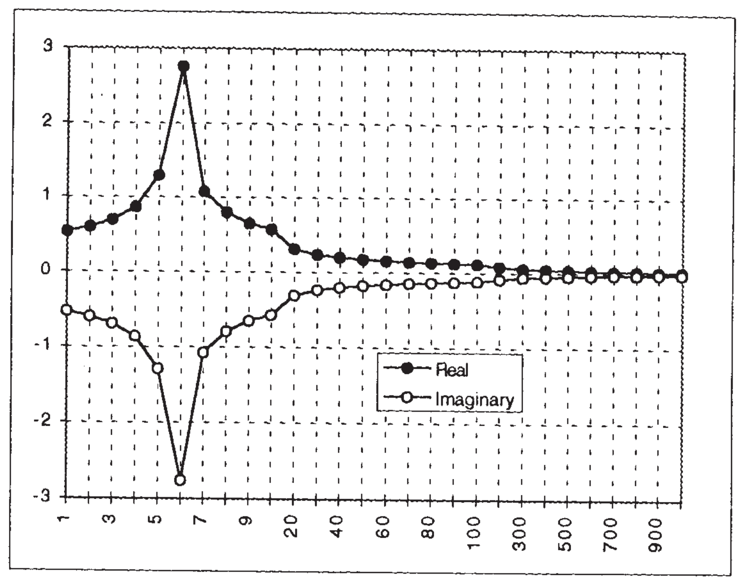

Table 5: Bellows Transverse Coupling Impedance (kohm/m)

Circumference	220.688	m	
Number of Bellows	**48**		
No. of Convolutions	**6**		
Height of Convolution	**25**	mm	
Width of Convolution	**10**	mm	
Pipe inner Radius	100	mm	
Pipe Cutoff	726	(n)	610.763268 MHz
$n-Q_{H,V}$	0.18		
Z/n @ n=1	-1.097841	ohm	
Capacitance / unit length	2.78162897	pF/cm	
Inductance / unit length	707.499103	pH/cm	
Characteristic Impedance	15.9482614	ohm	
Resistivity	**73**	µohm-cm	***stainless steel***
Wall Impedance	14.7988229	ohm/cm	
Q	0.67712062		
Shunt Impedance	13.7495824	ohm/convolution	
Lowest resonating mode	2522	(n)	2997.925 MHz
Z/n @ resonance	none	ohm	
relative freq. spread	**10**	%	
Z/n with freq. spreading	none	ohm	

n	Real	Imaginary
1	0	-1.8285178
2	0	-2.3071808
3	0	-3.1253152
4	0	-4.8424892
5	0	-10.747872
6	0	-48.962017
7	0	-7.4686902
8	0	-4.042628
9	0	-2.7713166
10	0	-2.1082842
20	0	-0.6213061
30	0	-0.3641829
40	0	-0.2574633
50	0	-0.1990174
60	0	-0.1621155
70	0	-0.1366873
80	0	-0.1180927
90	0	-0.1038964
100	0	-0.0926975
200	0	-0.0436981
300	0	-0.0275077
400	0	-0.0192103
500	0	-0.0140691
600	0	-0.0105418
700	0	-0.0079763
800	0	-0.0060472
900	0	-0.004571
1000	0	-0.0034332

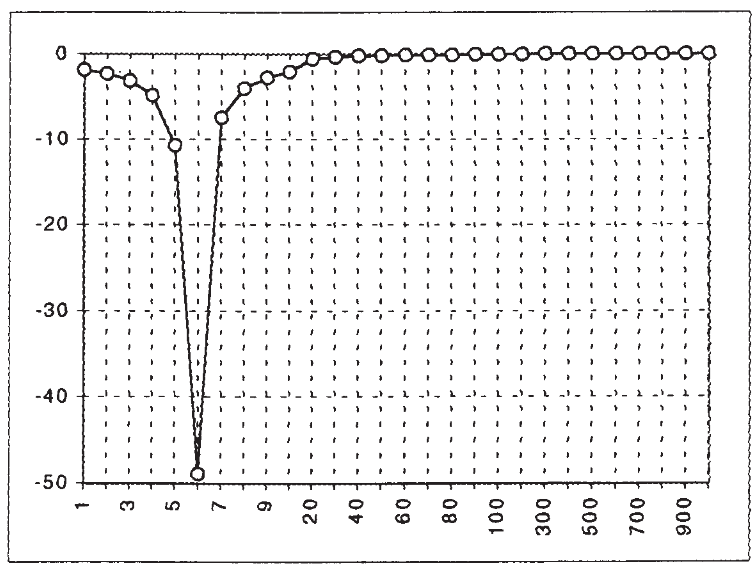

Table 6: Transverse Coupling Impedance of Beam Position Monitors (kohm/m)

Number	48		
No. of Plates	2		
Plate Length	20 cm		
Plate Width	7.5 cm		
Pipe Radius	10 cm		
Characteristic Impedance	50 ohm		
Circumference / π	70.2471722 m		
Z/n @ n=1	-0.3410463 ohm		
lowest resonating mode	315 (n)	374.740625 MHz	
pipe cutoff	726 (n)	610.763268 MHz	
	8.02799661		

n	Real	Imaginary
1	0.00283256	-0.5680229
2	0.01429586	-1.4333647
3	0.04356996	-2.9122199
4	0.12000912	-6.0157162
5	0.41615557	-16.687312
6	2.72970315	-91.206382
7	0.56669234	-16.227945
8	0.40058674	-10.036142
9	0.34750638	-7.7378307
10	0.32632651	-6.538571
20	0.38371468	-3.8346507
30	0.50396806	-3.3436096
40	0.62972541	-3.1150721
50	0.75491125	-2.9647231
60	0.87742891	-2.8445547
70	0.9960844	-2.7367194
80	1.11000244	-2.6332369
90	1.21846191	-2.5301622
100	1.32083892	-2.425467
200	1.92093514	-1.2406715
300	1.70406945	-0.1277024
400	0.99430127	0.44864582
500	0.31953794	0.42184866
600	0.01458806	0.09678546
700	0.05812594	-0.1596997
800	0.21178303	-0.1868996
900	0.27065975	-0.0617763
1000	0.19818697	0.05576117

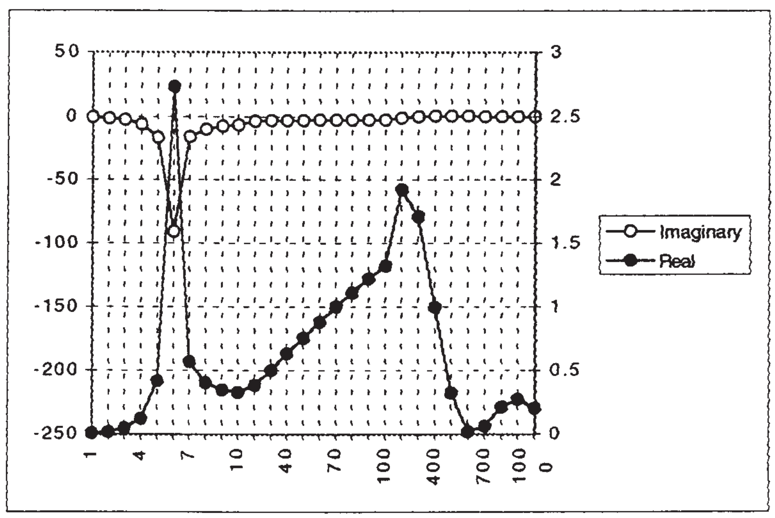

Table 7: Transverse Coupling Impedance (kohm/m) for the Damper System

Number of Systems	**1**		
Number of Plates	**2**		
Plate Length	**250**	cm	
Plate Width	**10**	cm	
Pipe radius, b	10	cm	
Permeability	**1**		
Dielectric	**10**		
Characteristic Impedance	**50**	ohm	
Circumference / π	70.2471722	m	8.02799661
lowest resonating mode	8	(n)	9.48027125 MHz
pipe cutoff	726	(n)	610.763268 MHz

n	Real	Imaginary
1	0.18480299	-0.8024333
2	0.89222894	-1.8354173
3	2.52326766	-3.132233
4	6.24693769	-4.9260537
5	18.8202215	-8.9469449
6	103.347533	-23.228792
7	17.2322139	-0.0008321
8	9.32748551	2.0750491
9	5.85303431	2.72067819
10	3.70386617	2.80179501
20	1.20782967	-0.2256991
30	0.14076986	0.28974365
40	0.59404071	0.53513965
50	0.55344516	0.03904205
60	0.20905178	0.16499447
70	0.43606552	0.29136964
80	0.44223769	-1.039E-16
90	0.21924859	0.0494186
100	0.35018403	0.13630465
200	0.10082392	-0.0629735
300	0.05338937	0.01007876
400	0.03458231	-4.785E-18
500	0.04670946	0.01424815
600	0.02432288	-0.0218694
700	0.00539045	0.01301315
800	0.02655752	1.2383E-17
900	0.0058601	-0.0046866
1000	0.00792132	0.00181693

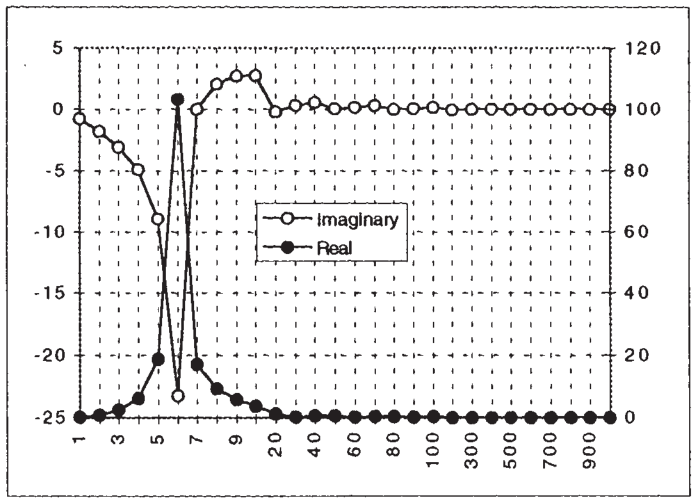

Table 8: Transverse Coupling Impedance (kohm/m) of the Kicker Magnets

Number of Systems	4		
Number of Plates	2		
Plate Length	40	cm	
Plate Width	10	cm	
Pipe radius, b	10	cm	
Permeability	1000		
Dielectric	1		
Characteristic Impedance	50	ohm	
Circumference / π	70.2471722	m	8.02799661
lowest resonating mode	5	(n)	5.92516953 MHz
pipe cutoff	726	(n)	610.763268 MHz

n	Real	Imaginary
1	1.61147923	-4.9596231
2	7.35664492	-10.125553
3	18.8786054	-13.71611
4	40.4242626	-13.134639
5	99.1935157	-6.074E-15
6	408.726456	132.803276
7	45.1149551	32.7779335
8	12.8902679	17.7419318
9	2.44237121	7.51684567
10	2.918E-31	2.3828E-15
20	3.4397E-31	1.4044E-15
30	4.5364E-31	1.2348E-15
40	5.7015E-31	1.1639E-15
50	6.8863E-31	1.1247E-15
60	8.0776E-31	1.0993E-15
70	9.27E-31	1.0814E-15
80	1.0461E-30	1.0678E-15
90	1.1648E-30	1.0568E-15
100	1.283E-30	1.0477E-15
200	2.4192E-30	9.8776E-16
300	2.9498E-29	2.7366E-15
400	4.2541E-30	8.6846E-16
500	9.7763E-29	3.5629E-15
600	4.5218E-29	2.0975E-15
700	1.8094E-29	1.1541E-15
800	5.3566E-30	5.4677E-16
900	6.4694E-31	1.652E-16
1000	9.5425E-29	1.7388E-15

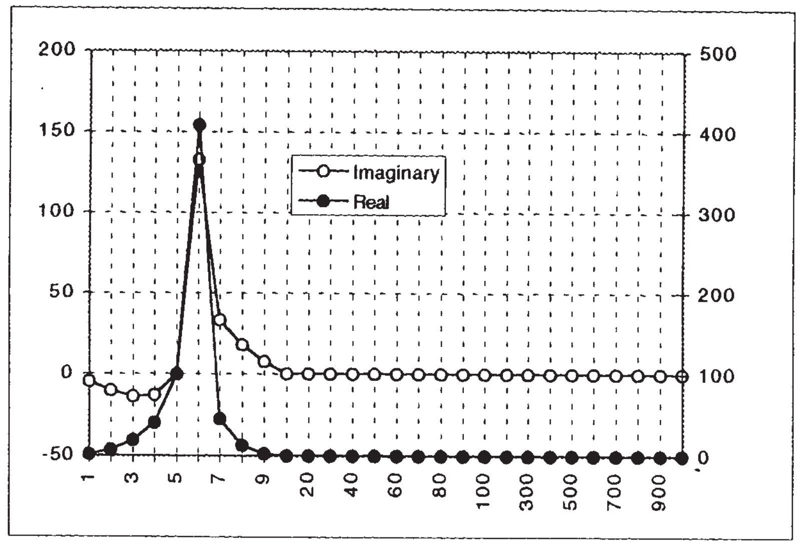

Table 9: Transverse Coupling Impedance of Vacuum Chamber Steps according to Hereward (kohm/m)

Number	**64**		
Pipe Radius inner	10 cm		
Pipe Radius outer	13 cm		
Cutoff mode	3678 (n)		4371.95251 MHz
Z/n below cutoff	0.62641946	-1.96795476 ohm	
Z/n @ cutoff	0.00489408	0 ohm	
pipe cutoff	726 (n)		610.763268 MHz
Circumference / π	70.2471722 m		8.02799661

n	Real	Imaginary
1	1.04333786	-3.27774256
2	2.63291842	-8.27155717
3	5.34984078	-16.8070205
4	11.0523449	-34.7219656
5	30.6632561	-96.3314602
6	167.624051	-526.606487
7	29.831031	-93.7169479
8	18.4535338	-57.9734862
9	14.2316232	-44.7099629
10	12.0297039	-37.7924294
20	7.0902474	-22.2746691
30	6.23399702	-19.5846792
40	5.87626233	-18.4608226
50	5.67788706	-17.8376083
60	5.55010914	-17.4361821
70	5.45948932	-17.1514915
80	5.39062194	-16.9351383
90	5.3354239	-16.7617285
100	5.28924745	-16.6166609
200	4.98676072	-15.6663708
300	4.7087096	-14.7928475
400	4.38450202	-13.7743193
500	4.01384951	-12.6098801
600	3.60903548	-11.3381194
700	3.18585396	-10.0086554
800	2.76040789	-8.67207714
900	2.34737448	-7.37449443
1000	1.9589471	-6.15421383

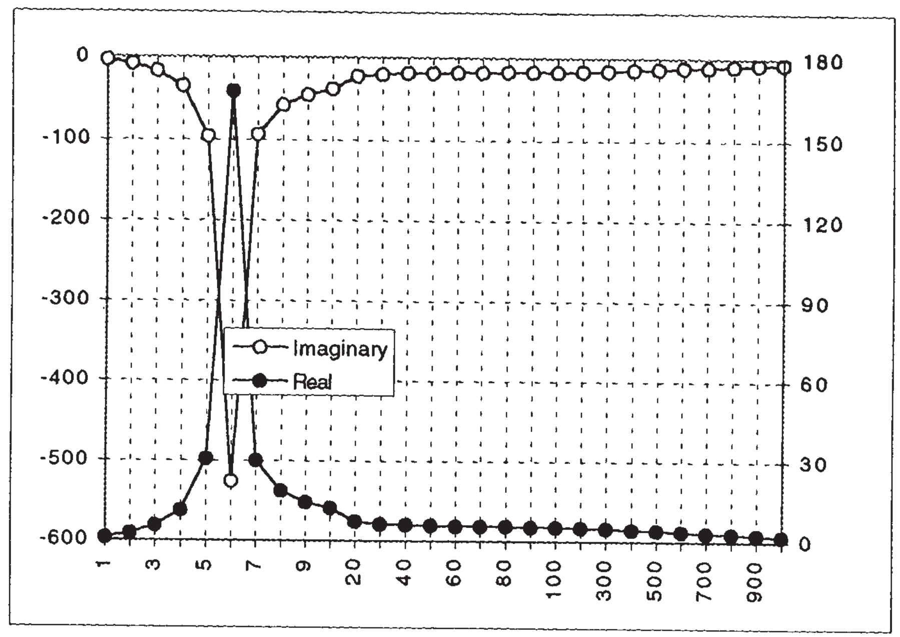

Table 10: Transverse Coupling Impedance of Vacuum Ports according to Sands (kohm/m)

Number	**48**	
diameter	**10** cm	
alpha	196.349541 cm^3	
cutoff mode	2207 (n)	2623.40924
coherence	**1**	
Pipe Radius	10 cm	
Z/n @ n=1	9.8561E-10 8.99357198 ohm	
Circumference / π	70.2471722 m	8.02799661

n	Real	Imaginary
1	1.6416E-09	14.9793132
2	3.3141E-08	37.8011493
3	2.2727E-07	76.8085511
4	1.1129E-06	158.680919
5	6.0307E-06	440.241068
6	5.6968E-05	2406.63964
7	1.6099E-05	428.297851
8	1.4866E-05	264.947923
9	1.6324E-05	204.333325
10	1.8927E-05	172.72052
20	8.9243E-05	101.816285
30	0.00026481	89.5434551
40	0.00059163	84.4353529
50	0.00111642	81.6225591
60	0.00188554	79.8306425
70	0.00294489	78.5794511
80	0.00433975	77.6477383
90	0.00611471	76.9193815
100	0.0083136	76.3275708
200	0.06251239	73.0586704
300	0.1981957	70.6946437
400	0.43431831	68.0255491
500	0.76942573	64.8156382
600	1.18205205	61.0074639
700	1.63499396	56.6227081
800	2.08234288	51.7401337
900	2.47765117	46.484396
1000	2.78152249	41.0133599

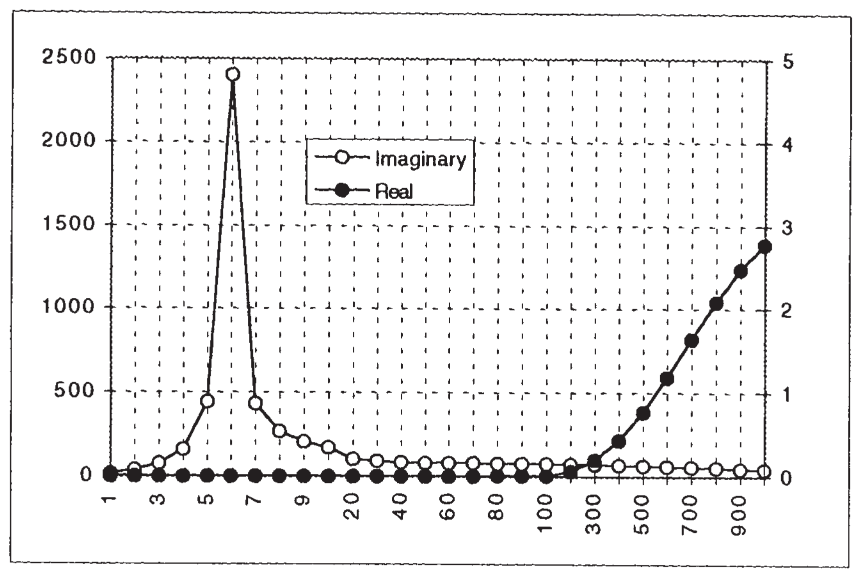

Table 11: Transverse Coupling Impedance (kohm/m) of the RF Cavity System

		System #1		System #2	
Number		6		2	
Harmonic Number		1		2	
Resonant Frequency		1.18867659 MHz		2.37735318 MHz	
Q		**2.00E+02**		**2.00E+02**	
Shunt Impedance		**0.008** Mohm		**0.008** Mohm	
Inductance		0.0053557 mH		0.00267785 mH	
Capacitance		3347.31381 pF		1673.65691 pF	
n		2		1	
omega	MHz	14.9373506		7.4686753	
denominator		9.0001		0.56250625	
Z/n @ n	ohm	0.2666637	79.9991111	0.1777758	-53.332741
Circumference / π		70.2471722 m	8.02799661		

n	Real	Imaginary
1	0.29609589	-88.828767
2	102.75504	336.246155
3	45.6813478	529.4909
4	35.2917106	517.544854
5	47.6344008	862.450404
6	146.698356	3172.85568
7	16.1805871	407.42781
8	6.6371203	190.780288
9	3.56997268	115.365222
10	2.18893677	78.5614103
20	0.15874279	11.3814407
30	0.04123481	4.43386923
40	0.01638104	2.3484097
50	0.00810015	1.4515232
60	0.00458093	0.98505238
70	0.00283724	0.71177997
80	0.00187657	0.53802566
90	0.00130439	0.42072338
100	0.00094262	0.3378191
200	0.00011107	0.07961175
300	3.1074E-05	0.0334091
400	1.2207E-05	0.01749851
500	5.7215E-06	0.01025226
600	2.9771E-06	0.00640156
700	1.655E-06	0.00415171
800	9.6064E-07	0.00275416
900	5.7373E-07	0.00185052
1000	3.4904E-07	0.00125089

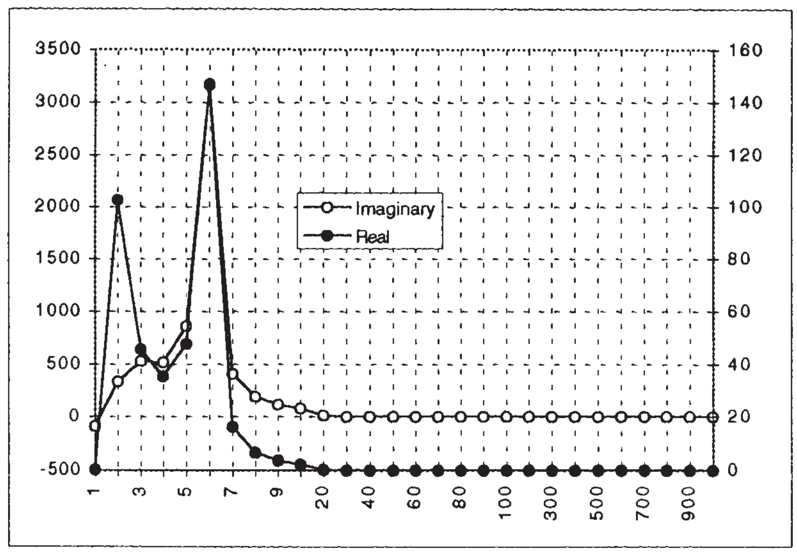

Table 12: Transverse Couplinmg Impedance of the various contributions. Real Part (kohm/m)

Real	n	Space Charge	Resistive	Bellows	BPM	Damper	Kicker	Steps	Vaccum Ports	RF Cavities	Total
	1	0	0.53443644	0	0.00283256	0.18480299	1.61147923	1.04333786	1.6416E-09	0.29609589	3.67298497
	2	0	0.60032532	0	0.01429586	0.89222894	7.35664492	2.63291842	3.3141E-08	102.75504	114.251453
	3	0	0.69870159	0	0.04356996	2.52326766	18.8786054	5.34984078	2.2727E-07	45.6813478	73.1753334
	4	0	0.86971649	0	0.12000912	6.24693769	40.4242626	11.0523449	1.1129E-06	35.2917106	94.0049826
	5	0	1.29569495	0	0.41615557	18.8202215	99.1935157	30.6632561	6.0307E-06	47.6344008	198.023251
	6	0	2.76546972	0	2.72970315	103.347533	408.726456	167.624051	5.6968E-05	146.698356	831.891626
	7	0	1.08008715	0	0.56669234	17.2322139	45.1149551	29.831031	1.6099E-05	16.1805871	110.005583
	8	0	0.79463077	0	0.40058674	9.32748551	12.8902679	18.4535338	1.4866E-05	6.6371203	48.5036399
	9	0	0.65791996	0	0.34750638	5.85303431	2.44237121	14.2316232	1.6324E-05	3.56997268	27.1024441
	10	0	0.57383978	0	0.32632651	3.70386617	2.918E-31	12.0297039	1.8927E-05	2.18893677	18.8226921
	20	0	0.31147062	0	0.38371468	1.20782967	3.4397E-31	7.0902474	8.9243E-05	0.15874279	9.15209439
	30	0	0.23840813	0	0.50396806	0.14076986	4.5364E-31	6.23399702	0.00026481	0.04123481	7.15864269
	40	0	0.20038942	0	0.62972541	0.59404071	5.7015E-31	5.87626233	0.00059163	0.01638104	7.31739055
	50	0	0.17610722	0	0.75491125	0.55344516	6.8863E-31	5.67788706	0.00111642	0.00810015	7.17156725
	60	0	0.15886102	0	0.87742891	0.20905178	8.0776E-31	5.55010914	0.00188554	0.00458093	6.80191731
	70	0	0.14578116	0	0.9960844	0.43606552	9.27E-31	5.45948932	0.00294489	0.00283724	7.04320253
	80	0	0.13540661	0	1.11000244	0.44223769	1.0461E-30	5.39062194	0.00433975	0.00187657	7.08448499
	90	0	0.12690492	0	1.21846191	0.21924859	1.1648E-30	5.3354239	0.00611471	0.00130439	6.90745843
	100	0	0.11976249	0	1.32083892	0.35018403	1.283E-30	5.28924745	0.0083136	0.00094262	7.0892891
	200	0	0.08106593	0	1.92093514	0.10082392	2.4192E-30	4.98676072	0.06251239	0.00011107	7.15220916
	300	0	0.06281087	0	1.70406945	0.05338937	2.9498E-29	4.7087096	0.1981957	3.1074E-05	6.72720606
	400	0	0.05077561	0	0.99430127	0.03458231	4.2541E-30	4.38450202	0.43431831	1.2207E-05	5.89849173
	500	0	0.04163717	0	0.31953794	0.04670946	9.7763E-29	4.01384951	0.76942573	5.7215E-06	5.19116553
	600	0	0.03420948	0	0.01458806	0.02432288	4.5218E-29	3.60903548	1.18205205	2.9771E-06	4.86421092
	700	0	0.02797766	0	0.05812594	0.00539045	1.8094E-29	3.18585396	1.63499396	1.655E-06	4.91234363
	800	0	0.02268769	0	0.21178303	0.02655752	5.3566E-30	2.76040789	2.08234288	9.6064E-07	5.10377996
	900	0	0.01819701	0	0.27065975	0.0058601	6.4694E-31	2.34737448	2.47765117	5.7373E-07	5.11974307
	1000	0	0.01441129	0	0.19818697	0.00792132	9.5425E-29	1.9589471	2.78152249	3.4904E-07	4.96098952

Table 13: Transverse Couplinmg Impedance of the various contributions. Imaginary Part (kohm/m)

Imagin.	n	Space Charge	Resistive	Bellows	BPM	Damper	Kicker	Steps	Vaccum Ports	RF Cavities	Total
	1	2406.85334	-0.5344364	-1.8285178	-0.5680229	-0.8024333	-4.9596231	-3.2777426	14.9793132	-88.828767	2321.03312
	2	2406.85236	-0.6003253	-2.3071808	-1.4333647	-1.8354173	-10.125553	-8.2715572	37.8011493	336.246155	2756.32626
	3	2406.85071	-0.6987016	-3.1253152	-2.9122199	-3.132233	-13.71611	-16.80702	76.8085511	529.4909	2972.75856
	4	2406.84841	-0.8697165	-4.8424892	-6.0157162	-4.9260537	-13.134639	-34.721966	158.680919	517.544854	3018.5636
	5	2406.84545	-1.2956949	-10.747872	-16.687312	-8.9469449	-6.074E-15	-96.33146	440.241068	862.450404	3575.52764
	6	2406.84183	-2.7654697	-48.962017	-91.206382	-23.228792	132.803276	-526.60649	2406.63964	3172.85568	7426.37128
	7	2406.83755	-1.0800872	-7.4686902	-16.227945	-0.0008321	32.7779335	-93.716948	428.297851	407.42781	3156.84664
	8	2406.83262	-0.7946308	-4.042628	-10.036142	2.0750491	17.7419318	-57.973486	264.947923	190.780288	2809.53092
	9	2406.82702	-0.65792	-2.7713166	-7.7378307	2.72067819	7.51684567	-44.709963	204.333325	115.365222	2680.88606
	10	2406.82077	-0.5738398	-2.1082842	-6.538571	2.80179501	2.3828E-15	-37.792429	172.72052	78.5614103	2613.89137
	20	2406.72207	-0.3114706	-0.6213061	-3.8346507	-0.2256991	1.4044E-15	-22.274669	101.816285	11.3814407	2492.652
	30	2406.55757	-0.2384081	-0.3641829	-3.3436096	0.28974365	1.2348E-15	-19.584679	89.5434551	4.43386923	2477.29375
	40	2406.32728	-0.2003894	-0.2574633	-3.1150721	0.53513965	1.1639E-15	-18.460823	84.4353529	2.3484097	2471.61244
	50	2406.03124	-0.1761072	-0.1990174	-2.9647231	0.03904205	1.1247E-15	-17.837608	81.6225591	1.4515232	2467.96691
	60	2405.66946	-0.158861	-0.1621155	-2.8445547	0.16499447	1.0993E-15	-17.436182	79.8306425	0.98505238	2466.04843
	70	2405.24197	-0.1457812	-0.1366873	-2.7367194	0.29136964	1.0814E-15	-17.151492	78.5794511	0.71177997	2464.65389
	80	2404.74881	-0.1354066	-0.1180927	-2.6332369	-1.039E-16	1.0678E-15	-16.935138	77.6477383	0.53802566	2463.1127
	90	2404.19001	-0.1269049	-0.1038964	-2.5301622	0.0494186	1.0568E-15	-16.761729	76.9193815	0.42072338	2462.05684
	100	2403.56563	-0.1197625	-0.0926975	-2.425467	0.13630465	1.0477E-15	-16.616661	76.3275708	0.3378191	2461.11273
	200	2393.72841	-0.0810659	-0.0436981	-1.2406715	-0.0629735	9.8776E-16	-15.666371	73.0586704	0.07961175	2449.77191
	300	2377.42244	-0.0628109	-0.0275077	-0.1277024	0.01007876	2.7366E-15	-14.792848	70.6946437	0.0334091	2433.1497
	400	2354.78052	-0.0507756	-0.0192103	0.44864582	-4.785E-18	8.6846E-16	-13.774319	68.0255491	0.01749851	2409.42791
	500	2325.98604	-0.0416372	-0.0140691	0.42184866	0.01424815	3.5629E-15	-12.60988	64.8156382	0.01025226	2378.58244
	600	2291.27052	-0.0342095	-0.0105418	0.09678546	-0.0218694	2.0975E-15	-11.338119	61.0074639	0.00640156	2340.97643
	700	2250.91048	-0.0279777	-0.0079763	-0.1596997	0.01301315	1.1541E-15	-10.008655	56.6227081	0.00415171	2297.34605
	800	2205.22381	-0.0226877	-0.0060472	-0.1868996	1.2383E-17	5.4677E-16	-8.6720771	51.7401337	0.00275416	2248.07899
	900	2154.56557	-0.018197	-0.004571	-0.0617763	-0.0046866	1.652E-16	-7.3744944	46.484396	0.00185052	2193.58809
	1000	2099.32343	-0.0144113	-0.0034332	0.05576117	0.00181693	1.7388E-15	-6.1542138	41.0133599	0.00125089	2134.22356

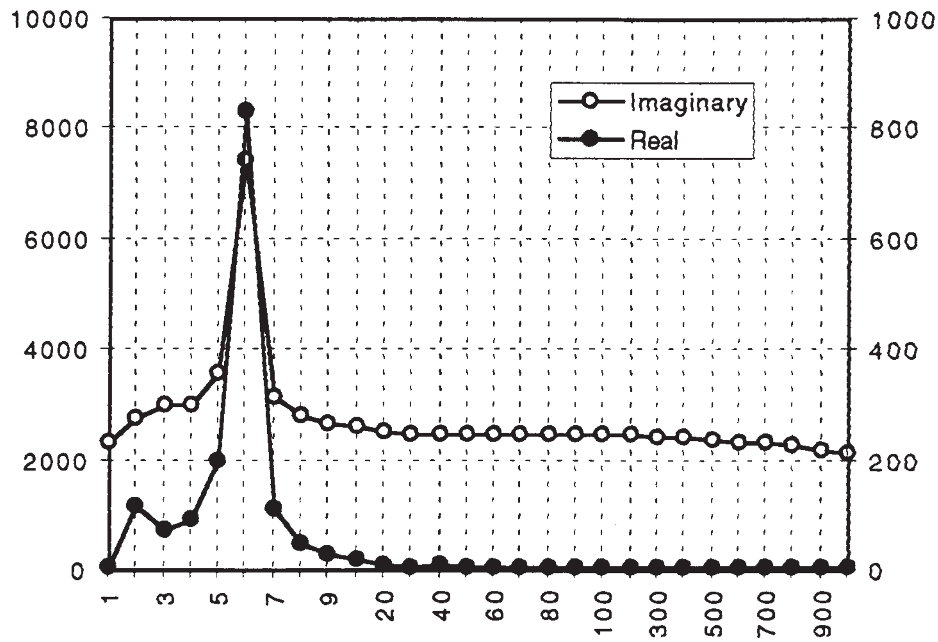

Figure 2. The Transverse Coupling Impedance Z_T (in kohm/m) vs. the Harmonic Number n

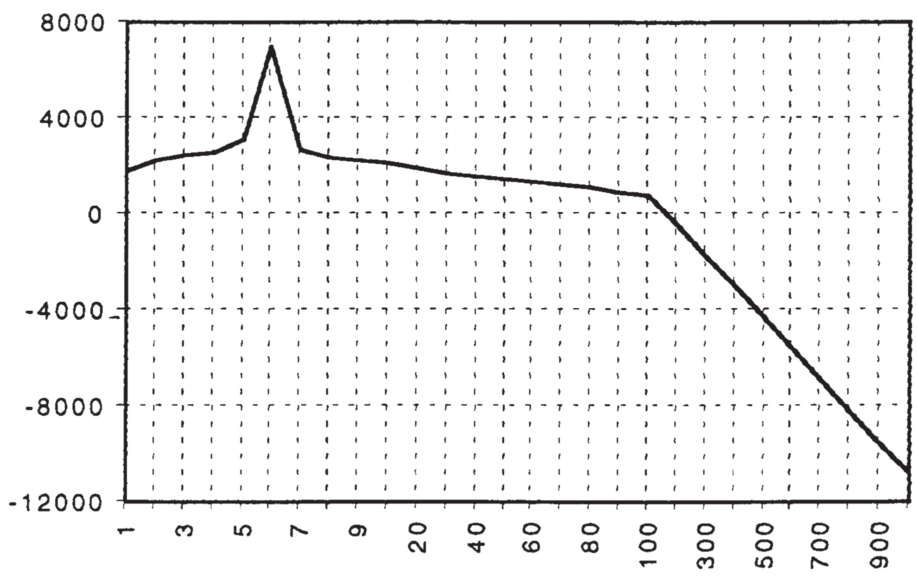

Figure 3. The difference $|Z_T| - Z_{beam}$ (in kohm/m) vs. the Harmonic Number n

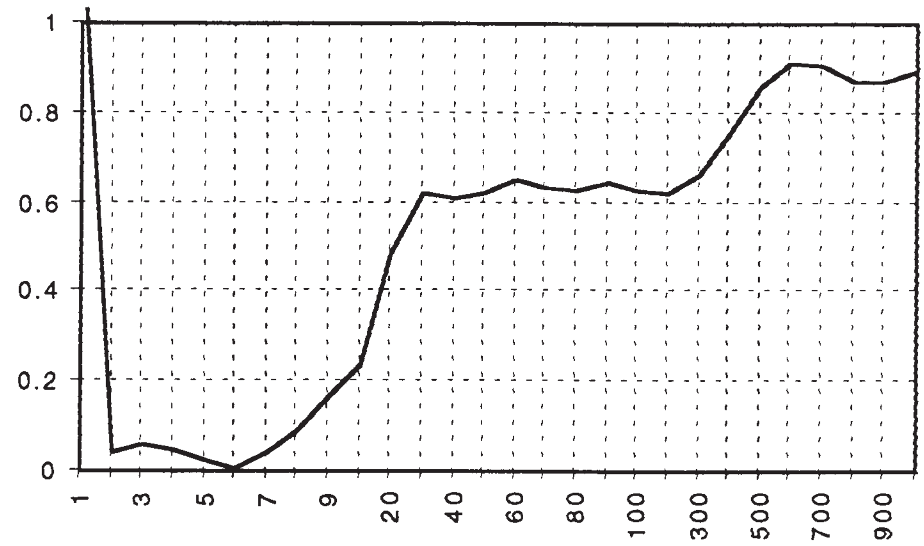

Figure 4. Growth time τ of the Instability (in ms) vs. the Harmonic Number n

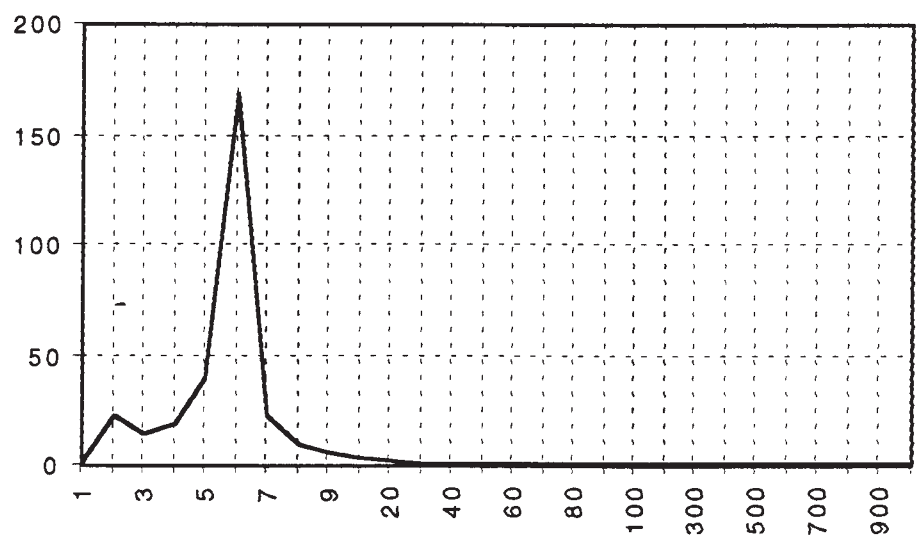

Figure 5. The ratio T_s / τ vs. the Harmonic Number n

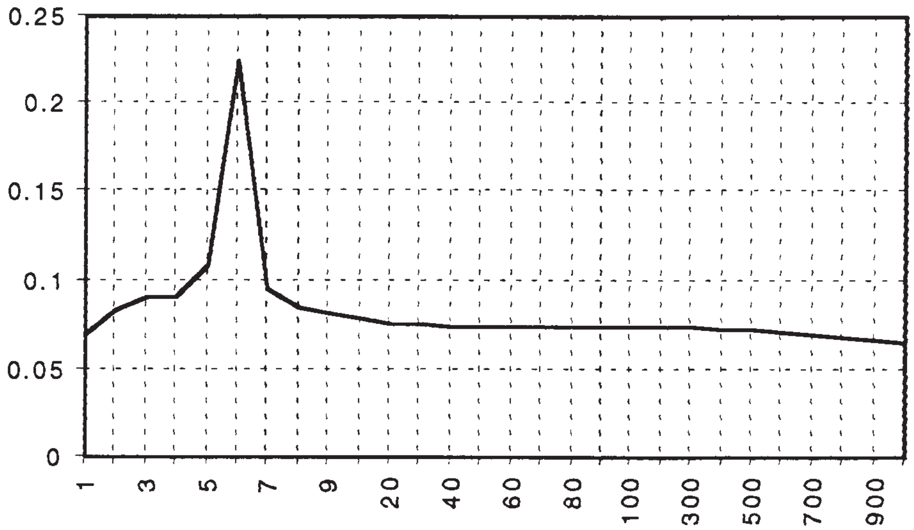

Figure 6. The Real Frequency-Shift $\Delta\omega / 2\pi f_0$ vs. the Harmonic Number n

How to Reduce the Growth Rate of the Instability

The results we have shown so far apply to the beam intensity at the end of the accumulation cycle, and for the reference betatron tunes $Q_{H,V} = 5.82$. The major concern is obviously the instability for those modes in proximity of the betatron tune. The fewer modes below n = 6 are not relevant in this analysis, since they cannot be excited by the beam. the worst case is represented by the mode n = 6. All the modes n > 20 have growth times of at least half a millisecond, can be easily Landau-damped with a betatron tune spread of 0.1 or less, and thus have no significant consequences to the beam performance.

Inspection of Table 12 shows that the imaginary part of the transverse coupling impedance is essentially given by the space-charge term. The contribution from the other components are entirely negligible. But the largest contribution to the resistive part of the impedance at n = 6 comes (in the order) from the kicker magnets (409 kohm/m), the vacuum chamber steps (168 kohm/m), the RF cavities (147 kohm/m), and the active damper system (103 kohm/m). The contribution from the wall resistivity is very small (2.8 kohm/m) when compared to the other components. This makes one wonder whether there is indeed any need to reconsider the choice of the vacuum chamber material. For instance, for a 100% stainless steel vacuum chamber, the contribution of the wall resistivity increases to only 12.3 kohm/m, still quite small compared to the contribution of the other components. At the same time the resistive contribution of the beam position monitor is only 2.7 kohm/m.

Lowering the betatron tune from 5.8 to 5.2 causes an increase of the instability grow time by a factor of four. At n = 6 now $\tau = 21\ \mu s$. Though this is a significant improvement, nevertheless clearly is not enough. We have pointed out that there are four major components which need very careful engineering design to lower their resistive contribution. One extreme approach is to assume that they have no resistive contribution. The results are shown in Table 14. We compare two values of betatron tunes, two cases of vacuum chamber material and the contribution of the four major components included (Yes) or not (No).

Table 14: Instability Growth Time τ (in ms) at n = 6

Betatron Tune $Q_{H,V} = 5.82$				Betatron Tune $Q_{H,V} = 5.20$			
Stainless Steel		Aluminum		Stainless Steel		Aluminum	
Yes	No	Yes	No	Yes	No	Yes	No
0.0053	0.295	0.0053	0.868	0.021	0.615	0.021	2.06

References

[1] Y.Y. Lee, "The 4 Fold Symmetric lattice for the NSNS Accumulator Ring", BNL/NSNS Technical Note No. 26. February 19, 1997.

[2] L.J. Laslett, V.K. Neil, A.M. Sessler, Rev. Sci. Instr., 36, 436, (1965).

[3] K. Hubner, A.G. Ruggiero, V.G. Vaccaro, Proc. 7th Int. Conf. on High Energy Accel., Yerevan, p. 343, (1969).

[4] F. Sacherer, Proc. of 9th Int. Conf. on High Energy Accele., SLAC, p. 347, (May 1974).

[5] A.G. Ruggiero, "The Longitudinal Coupling Impedance in the NSNS Accumulator Ring", BNL/NSNS Technical Note No. 27. April, 1997.

[6] H. Hereward, CERN / ISR - DI / 75-47 (Oct. 1975).

[7] Yong Ho Chin, "User's Guide for ABCI. Version 8.7", CERN SL/94-02 (AP), Feb. 1994.

[8] A.G. Ruggiero and V.G. Vaccaro, "The Electro-Magnetic Field of an Intense Coasting Beam Perturbation in the Presence of Conductive Plates terminated at both Ends", Internal Report LNF-69/70, Frascati (Italy), Nov. 1969.